

# Photocathode microwire monitor for nondestructive and highly sensitive spatial profile measurements of ultraviolet, x-ray, and charged particle beams

Masaki Hori

CERN, CH-1211 Geneva 23, Switzerland and Department of Physics, University of Tokyo,  
7-3-1 Hongo, Bunkyo-ku, Tokyo 113-0033, Japan

(Received 8 July 2005; accepted 3 October 2005; published online 23 November 2005)

A nondestructive and sensitive monitor consisting of photocathode wire grids arranged in an  $XY$  configuration for measuring the spatial profile, divergence, and intensity of pulsed UV, x-ray, and charged particle beams is described. The monitor has been used to measure laser beams at wavelengths  $\lambda=213$ – $532$  nm, and antiproton, proton,  $H^-$  ions, and electron beams of energies  $E=50$  eV to 5 MeV. © 2005 American Institute of Physics. [DOI: 10.1063/1.2130931]

## I. INTRODUCTION

We describe here a microwire monitor that measures nondestructively the spatial profile, divergence, and intensity of UV, x-ray, and charged particle beams. It can detect (i) single, extremely weak light pulses intercepted by its photocathode wires (Fig. 1), with energies down to  $E\sim 5$  pJ and  $E<0.1$  pJ at the respective wavelengths  $\lambda=213$  and 20 nm, which correspond to the emission of  $\sim 500$ – $1000$  photoelectrons from the individual wires on average, (ii) pulsed beams containing  $\sim 500$ – $5000$  charged particles that strike the individual wires and produce secondary electrons, or (iii) charged particle beams of low kinetic energy that stop and deposit their charge in the wires. The monitor had spatial and timing resolutions  $\Delta x=0.25$ – $1$  mm and  $\Delta t\sim 0.5$ – $10$   $\mu$ s, and was operated in ultrahigh vacuum ( $p\sim 10^{-8}$  Pa), low temperatures ( $T<100$  K), and strong magnetic fields ( $B>0.1$  T).

The profiles of such low-intensity beams are often measured using phosphor screens, microchannel plates, or charged-coupled devices<sup>1,2</sup> (CCDs) that intercept and destroy all of the beam. By contrast, the photocathode wires of the monitor described here intercepted only 1%–4% of the beam, while the remaining 96%–99% passed without degradation. The divergence of a single beam pulse could be determined using two such monitors to measure its profile at two positions simultaneously along the beam path. Profile monitors with wire<sup>3–6</sup> and strip<sup>7–9</sup> electrodes have been used for many years in particle accelerators to measure high-intensity beams [e.g., containing  $\sim 10^{12}$  protons of energy  $E=120$  GeV,<sup>3</sup>  $\sim 10^{10}$  electrons with  $E=50$  GeV,<sup>4</sup> or UV synchrotron radiation produced by GeV-scale electrons<sup>5</sup> of current  $I\sim 180$  mA], but the present one employs sensitive electronics to measure beam intensities that are lower by 5–7 orders of magnitude.

The monitor was recently used in laser spectroscopy experiments on antiprotonic helium atoms ( $\bar{p}\text{He}^+$ )<sup>10</sup> and ions ( $\bar{p}\text{He}^{2+}$ )<sup>11</sup> carried out at the Antiproton Decelerator of CERN. In a previous series of experiments,<sup>12</sup> profile monitors with parallel-plate electrodes made of metallized polyester

foils were placed in an antiproton beam of energy  $E=5$ – $21$  MeV. The antiprotons had such high kinetic energy that they traversed the foil electrodes with negligible energy loss and multiple scattering, and this allowed the beam profile to be nondestructively measured. The latest experiments,<sup>10,11</sup> however, used antiprotons of much lower energy ( $E<100$  keV) emitted from a radio frequency quadrupole decelerator.<sup>13</sup> The parallel-plate monitor could no longer be used because the antiprotons would stop in it. We therefore developed the wire monitor described here, which allowed most of the low-energy antiprotons to pass through without any degradation, while the small portion intercepted by the wires produced the signal. The monitor was used to measure antiproton beams of energies between  $E=25$  keV and 5.3 MeV.

## II. MONITOR CONSTRUCTION

### A. Photocathode wires and vacuum chamber

The monitor consisted of two position-sensitive photocathode grids providing the  $X$  and  $Y$  projections of the beam, sandwiched between three anode grids with a distance  $l=2$  mm between them (Fig. 1). Each grid consisted of 32 gold-coated tungsten wires of diameter  $d=5$ – $10$   $\mu$ m stretched over a ceramic frame, with a pitch  $\Delta x=0.25$ – $1$  mm between neighboring wires [Figs. 2(a) and 2(b)]. They were manufactured by first printing a pattern of 32 gold readout microstrips with thickness  $t_r=30$   $\mu$ m along the edges of a ceramic frame, which measured 100 mm  $\times$  90 mm  $\times$  2 mm and had a 50 mm  $\times$  50 mm opening in the center to allow the passage of the beam. Gold-coated tungsten wires were stretched over the frame with a mechanical tension  $g=10$ – $20$  g. The two ends of each wire were aligned and pressed onto the corresponding microstrips with several hundred grams of force, using an electrode tip made of tungsten. The wires were then embedded and fused into the microstrips by applying a pulsed current on the tip. Two rows of spring-loaded sockets with diameter  $d=1$  mm made of copper-beryllium were soldered onto the microstrips along the edges of the frame using a fluxless, gold-tin solder.

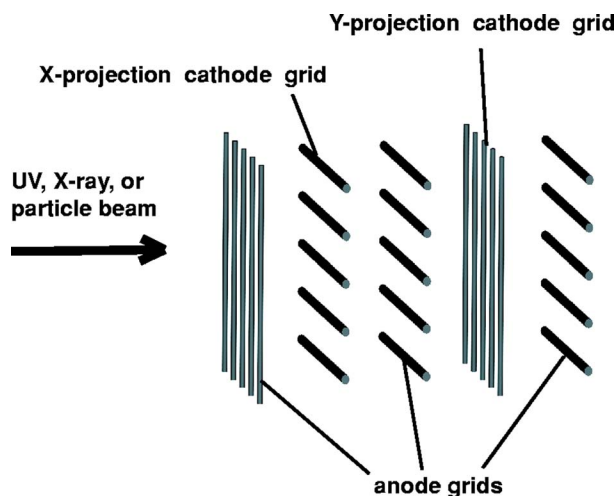


FIG. 1. Configuration of the two position-sensitive cathode and three anode grids of the microwire monitor.

The grids were allowed to stand for 24 h, to verify that none of the bonded wires would spontaneously break off. Whereas wires of diameters  $d=5\text{--}30\ \mu\text{m}$  diam could be reliably bonded, those with larger diameters  $d\geq 100\ \mu\text{m}$  often broke off because of the higher mechanical tension in them. The measurements described below were carried out using electrodes with  $d=10\ \mu\text{m}$ , resolution  $\Delta x=1\ \text{mm}$ , active area  $xy=32\times 32\ \text{mm}$ , and optical transmission of  $\sim 98\%$ .

The grids were baked in vacuum at temperature  $T\sim 100\ ^\circ\text{C}$  to remove outgassing contamination (mostly water) from their surfaces, thereby allowing them to be used in ultrahigh vacuum  $p\sim 10^{-8}\ \text{Pa}$ . Baking at higher temperature  $T>150\ ^\circ\text{C}$  caused some of the tungsten wires to break off, presumably because they (having a thermal expansion  $\theta\sim 5\times 10^{-6}\ \text{K}^{-1}$ ) were stretched by the ceramic frame ( $\theta\sim 9\times 10^{-6}\ \text{K}^{-1}$ ). It should be possible to safely bake grids mounted on ceramics with smaller  $\theta$  values (e.g., silicon nitride or silicon carbide) to even higher temperatures ( $T\sim 200\ ^\circ\text{C}$ ). The grids were quite robust and easy to handle; some 20 units, with a total of 600 wires, were placed in small plastic packages and safely shipped from Japan to Switzerland by normal airmail. Over a 6-yr period during which they were repeatedly evacuated, baked, and exposed to air, only a few wires broke off spontaneously.

The vacuum chamber was a  $120\ \text{mm}\times 120\ \text{mm}\times 60\ \text{mm}$  rectangular tube made of type 316L stainless steel, with 203-mm-diam Conflat vacuum flanges welded on both ends. The signals induced on the photocathode wires were transmitted through the chamber walls by a series of 140 L-shaped copper-beryllium pins of diameter  $d=1\ \text{mm}$  and length  $l=20\ \text{mm}$ . The pins were brazed with a pitch  $p=2.5\ \text{mm}$  into four sets of  $90\ \text{mm}\times 9\ \text{mm}\times 5\ \text{mm}$  ceramic seals, which were in turn precisely aligned and brazed onto the sides of the vacuum chamber, so that the pins formed a rectangular pattern along its inner circumference as shown in Figs. 2(a) and 2(b). The X- and Y-position-sensitive grids could be quickly mounted by connecting the rows of sockets on them with their pin counterparts on the chamber.

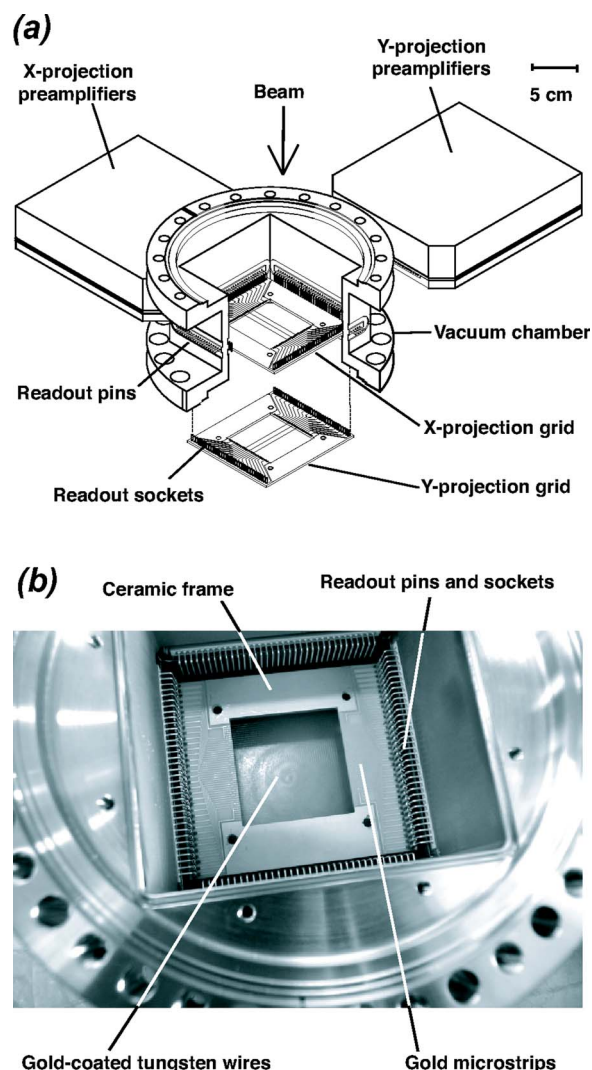


FIG. 2. Schematic drawing of the (a) photocathode microwire monitor and (b) photograph of its interior with a grid installed.

## B. Readout electronics

The photocathode grids (biased at  $-50\ \text{V}$ ) were irradiated by the beam, and the photoelectrons or secondary electrons emitted from them were accelerated toward the anode grids (at ground potential). The beam profile was obtained by using charge-sensitive preamplifiers to measure the charge  $Q_i$  ejected from each of the 64 wires on the X and Y photocathode grids with high sensitivity [Fig. 3]. Four sets of  $160\ \text{mm}\times 140\ \text{mm}\times 40\ \text{mm}$  sealed cases made of copper, each containing 16 preamplifiers (Clear Pulse hybrid integrated circuit CS515-2), were mounted on the sides of the chamber and provided the 64 readout channels. The signals were processed in these boxes in the following sequence: (i) Each preamplifier was connected to a photocathode wire through a decoupling capacitor  $C_d=2.7\ \text{nF}$ , and had a feedback capacitor and resistor of  $C_f=0.5\ \text{pF}$  and  $R_f=5\ \text{G}\Omega$ . The amplitude  $V_o$  of its output signal was related to the input charge  $Q_i$  by a conversion ratio  $dV_o/dQ_i\sim 2\ \text{V/pC}$ . (ii) A resistor-capacitor (RC) high-pass filter with a time constant  $\tau_p=50\ \mu\text{s}$  was used to differentiate the signal and avoid pile-up effects at high rates of the beam pulses. (iii) A transconductance amplifier converted the voltage signal  $V_o$

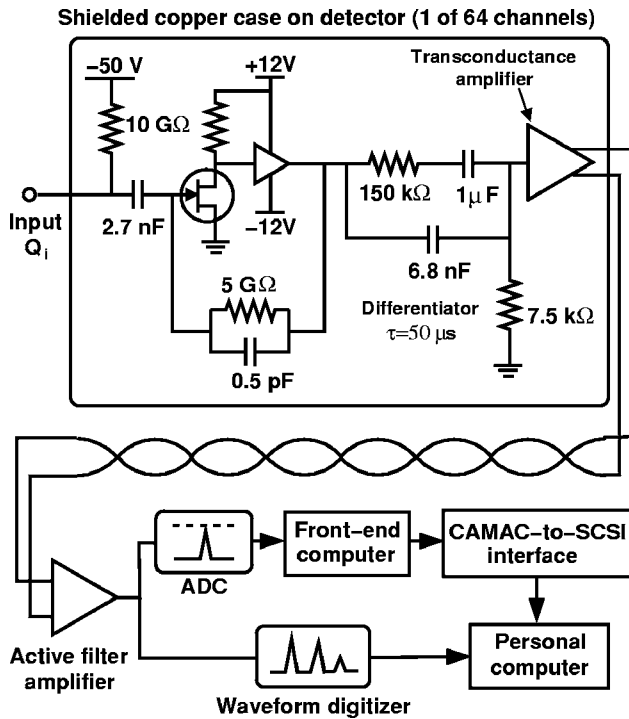


FIG. 3. Layout of the readout electronics of the microwire monitor.

into a differential current one  $I_d$  with a conversion ratio  $dI_d/dV_o = 3 \times 10^{-2}$  A/V. (iv) The signals were transmitted from the copper case to active filter amplifiers housed in a nearby electronic rack, over several meters of shielded twisted-pair cables with impedance  $R = 200 \Omega$ . The differential nature and low impedance of the signal ensured that any external electromagnetic interference picked up on the cable would not degrade the signal-to-noise ratio; this was important because the monitor was used in particle accelerators that contained high-power radio frequency systems operating at frequencies  $f = 10\text{--}200$  MHz.

The active filter amplifiers (Clear Pulse 4026 with custom modifications) each consisted of a differentiator and four integrators, which shaped the signal into Gaussian pulses with a peak time constant  $\tau_p = 2 \mu\text{s}$ . The amplitudes of these pulses, which were proportional to the number of photoelectrons emitted from each wire, were measured using peak-sensing analog-to-digital converters (ADCs, Hoshin C-008) with a resolution of 12 bits. A front-end computer (Kinetic Systems K3976 with a Motorola 68EC030 processor running at clock frequency  $f = 40$  MHz) read out the ADC values via Computer Automated Measurement and Control (CAMAC) interface at speeds of  $\sim 20\,000$  readings/s;<sup>14</sup> this allowed us to record the profiles of individual beam pulses arriving at rates up to  $f_r \sim 300$  Hz. Once the 4-Mbyte memory of the front-end computer was filled, the data was transferred to a personal computer (PC) via CAMAC-to-Small Computer System Interface (SCSI) interface (Kinetic Systems K3929). Beams arriving at higher rates  $f_r \sim 20$  kHz could be measured using an alternate readout method wherein the outputs of the active filter amplifiers were recorded with wave form digitizers of bandwidth  $f = 10\text{--}100$  MHz and resolution of 8 bits. Once the 1-Mbyte memory of the digitizers were filled, the data (corresponding to a 10–100 ms long wave form)

were transferred to the PC, and the peak heights of all the pulses recorded in each readout channel were measured to obtain the spatial beam profile. Still higher rates ( $f_r > 100$  kHz) could be measured by decreasing the time constants and gain of the pre- and active filter amplifiers, but this resulted in a lower sensitivity of the monitor. The PC was running the Linux operating system and the National Instruments Labview data acquisition software, and displayed the horizontal and vertical profiles of the beam. The same image could be simultaneously transmitted via network to several other PCs and workstations.

The rms equivalent noise charge  $\varepsilon$  (i.e., the signal charge for which the signal-to-noise ratio is unity) of an ideal detector at temperature  $T \sim 300$  K can be estimated using the equation,<sup>15</sup>

$$\varepsilon^2 = (C_{\text{det}} + C_{\text{amp}})^2 \left( \frac{a_1 8kT}{3t_p g_m} + \frac{a_2 K_f}{C_{\text{amp}}} \right) + a_3 t_p \left( 2eI_{\text{det}} + \frac{4kT}{R_f} \right), \quad (1)$$

where the Boltzmann constant and electric charge are denoted by  $k$  and  $e$ . The following techniques were used to minimize the noise: (i) The photocathode wires and preamplifiers were mounted on ceramic and Teflon substrates in close proximity ( $l = 50$  mm) to each other. This gave low values of the detector leak current  $I_{\text{det}} < 10$  pA and capacitance  $C_{\text{det}} \sim 10$  pF. (ii) Junction field-effect transistors with a low  $1/f$  noise coefficient  $K_f \sim 10^{-27}$  J and input capacitance  $C_{\text{amp}} \sim 10$  pF, a high transconductance  $g_m \sim 50$  mS, and large feedback resistors  $R_f = 5$  GΩ were used in the preamplifiers. (iii) Optimum values of the shaping peak time constant  $\tau_p \sim 2 \mu\text{s}$  and coefficients  $a_1\text{--}a_3$  close to unity were used.

The noise level of the monitor  $\varepsilon$  was calibrated absolutely against the signal produced by a  $p$ - $i$ - $n$  silicon detector irradiated with 59.5-keV x-rays from a <sup>241</sup>Am source. The measured noise,  $\varepsilon \sim 200$  electrons, was within a factor of 2 of the best values reported for any room-temperature detector of comparable capacitance. This implies that a wire irradiated with laser pulses of energy  $E \sim 10$  and  $\sim 0.1$  pJ at the respective wavelengths  $\lambda = 213$  and 20 nm would produce a signal-to-noise ratio of  $\sim 5$ , assuming quantum efficiencies  $\gamma \sim 1 \times 10^{-4}$  and  $\sim 8\%$ .<sup>16,17</sup>

### III. MEASUREMENTS AND RESULTS

The experimental setup (Fig. 4) involved two monitors positioned  $l = 2$  m apart along a beamline evacuated to pressure  $p = 10^{-7}$  Pa. Two injection-seeded Nd:yttrium aluminum garnet (YAG) lasers (Coherent Infinity) with beta barium borate (BBO) crystals cut for type-I frequency conversion were used to produce 1–3 ns long laser pulses with wavelengths  $\lambda = 213, 266, 355,$  and 532 nm. The 213-nm laser light of energy  $E = 30$  mJ was produced<sup>18</sup> by (i) using a 9-mm-long BBO crystal to frequency double the Nd:YAG laser beam of wavelength  $\lambda = 1064$  nm and energy  $E = 600$  mJ, (ii) further doubling the resulting 532-nm second harmonic light of  $E = 300$  mJ in an 8-mm-long crystal, thus generating a 266-nm fourth harmonic beam of  $E = 100$  mJ, (iii) mixing this with the 1064-nm fundamental

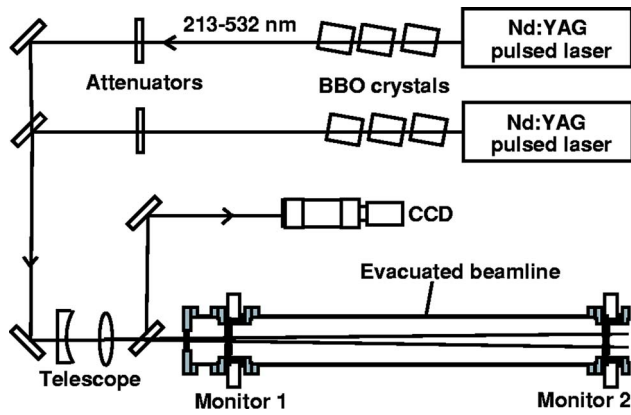


FIG. 4. Experimental layout to measure the profiles of two laser pulses with wavelengths  $\lambda=213\text{--}532$  nm.

light in a 7-mm-long crystal. The laser beams entered the beamline through a fused silica window, and telescopes were used to vary their diameters between  $d=5$  and 30 mm at the positions of the monitors. The laser energies were attenuated using dichroic beam splitters, and measured using pyroelectric or silicon diode detectors.<sup>19</sup> In Figs. 5(a)–5(d), the X and Y profiles of a single laser pulse of wavelength  $\lambda=266$  nm measured simultaneously by the two monitors are shown. The individual wires intercepted a laser energy  $E\sim 3$  nJ on average. The results are consistent with a beam divergence  $\Theta\sim 2$  mrad.

In Figs. 6(a)–6(d), the number of photoelectrons emitted from a wire irradiated with laser pulses of wavelengths  $\lambda=213\text{--}532$  nm and energies  $E=5$  pJ to 10  $\mu\text{J}$  is shown. At  $\lambda=213$  nm, the monitor showed a linear response and was sensitive to a minimum laser energy  $E_{\min}\sim 5$  pJ. The measured quantum efficiency  $\gamma\sim 8\times 10^{-5}$  agreed within a factor of 2 with experimental values.<sup>16</sup> At  $\lambda=266$  nm, the  $\gamma$  value

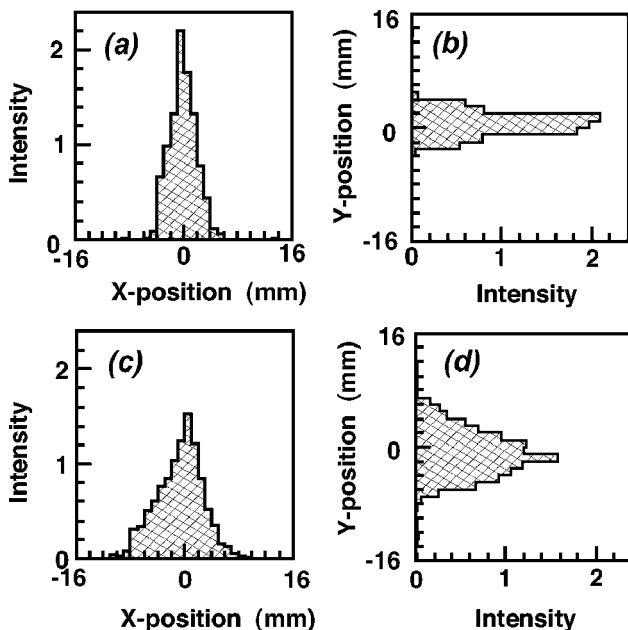


FIG. 5. Typical X and Y profiles of a laser pulse of wavelength  $\lambda=266$  nm and energy  $E\sim 3$  nJ intercepted by the individual wires on average, measured simultaneously by the (a)–(b) upstream and (c)–(d) downstream monitors.

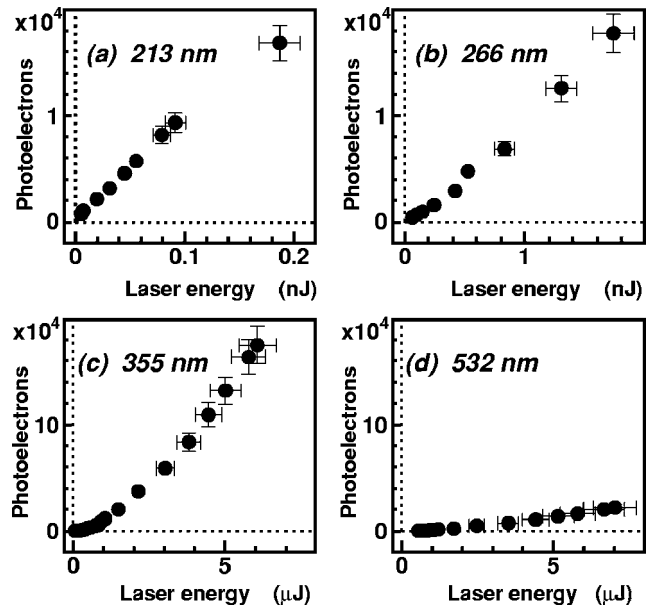


FIG. 6. Photoelectron yield from a photocathode wire irradiated with laser pulses of various energies and wavelengths (a)  $\lambda=213$ , (b) 266, (c) 355, and (d) 532 nm. Note different scales in the X and Y axis.

decreased to  $\sim 7\times 10^{-6}$ . At longer wavelengths  $\lambda=355$  and 532 nm, a nonlinear response was observed and the efficiency decreased by 3–4 orders of magnitude to  $\gamma=10^{-9}\text{--}10^{-8}$ ; the minimum laser energies that could be detected were  $E_{\min}\sim 0.1\text{--}0.5$   $\mu\text{J}$ , which here corresponded to power densities  $\rho\sim 50\text{--}200$   $\text{kW}/\text{cm}^2$ . This is due to the fact that since the 3.5 and 2.3 eV photon energies are now smaller than the  $\sim 4.6\text{-eV}$  work function of gold, photoelectron emission can only proceed via the nonlinear, simultaneous absorption of several photons.<sup>20</sup> This insensitivity against visible light may be useful in measuring weak UV laser beams mixed with a background of strong visible laser light, e.g., those produced by high-order harmonic generation.<sup>21</sup>

In Fig. 7, the timing and spatial response of the monitor

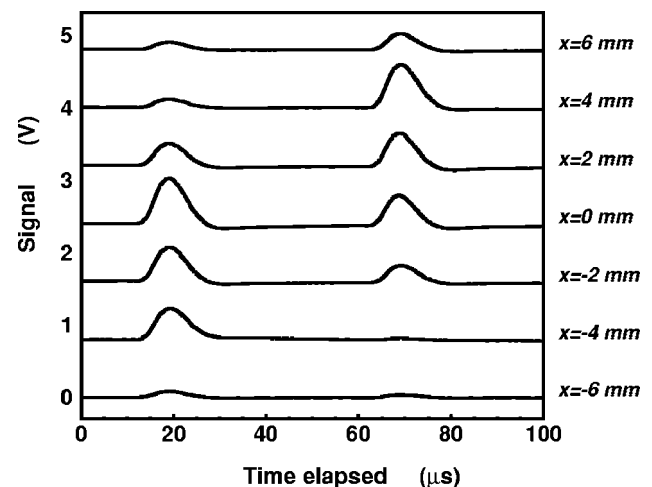


FIG. 7. Spatial and timing response of two laser pulses emitted sequentially by two Nd:YAG lasers, with wavelength  $\lambda=266$  nm and energy  $E\sim 1$  nJ intercepted by the individual wires, and arriving at a timing interval  $\Delta t=50$   $\mu\text{s}$ . The position of the first beam was horizontally shifted by 3 mm with respect to the second one (see text).

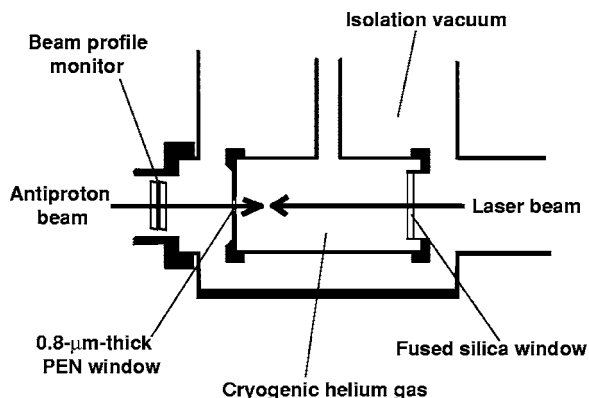


FIG. 8. Layout of the laser spectroscopy experiment of  $\bar{p}\text{He}^+$  and  $\bar{p}\text{He}^{2+}$ , wherein the wire monitor is used to measure the profiles of antiproton and laser beams.

against two laser pulses emitted sequentially by the two Nd:YAG lasers, arriving with a very short interval ( $\Delta t = 50 \mu\text{s}$ ), wavelength  $\lambda = 266 \text{ nm}$ , diameter  $d = 5 \text{ mm}$ , and energy  $E \sim 1 \text{ nJ}$  intercepted by the individual wires are shown. These were obtained by simultaneously recording the analog wave form of the signal from each wire comprising the X-projection grid using the wave-form digitizers described above. In order to study both the spatial and timing resolutions of the monitor, we shifted the position of the first laser beam by 3 mm relative to the second one. The measurement results (Fig. 7) clearly show that the two beams are indeed separated by 3 mm, and also agree with separate measurements using a CCD camera. The spectra were measured with a  $\tau_p = 2 \mu\text{s}$  time constant of the amplifier, but by decreasing this to  $\tau_p = 80 \text{ ns}$ , we resolved laser pulses arriving at intervals  $\Delta t \sim 0.5 \mu\text{s}$ .

The monitor was also used to measure charged particle beams, including (i) protons and  $\text{H}^-$  ions of energy  $E = 5\text{--}60 \text{ keV}$  produced by a duoplasmatron ion source, (ii) 5-MeV protons ejected from a linear accelerator, and (iii) 0.1–20 keV electrons emitted by an electron gun. A single particle striking a gold-coated wire can liberate between  $\gamma_e \sim 0.1$  and 2 secondary electrons depending on its type and energy.<sup>22</sup> In addition, particles with low kinetic energy (e.g. 1-MeV protons) stopped and deposited their charge in the wire. These processes enabled the monitor to detect weak beam pulses wherein on average  $\sim 500\text{--}5000$  particles struck the individual wires.

The fact that the monitor can nondestructively measure both laser and charged particle beams was used in the laser spectroscopy experiment of  $\bar{p}\text{He}^+$  atoms and  $\bar{p}\text{He}^{2+}$  ions described above, the layout of which is shown in Fig. 8. Here, 100-ns-long beam pulses containing  $(2\text{--}5) \times 10^6$  antiprotons of energy  $E = 60\text{--}100 \text{ keV}$  arrived at the monitor with a repetition rate  $f = 0.01 \text{ Hz}$ . Antiprotons emerging from the other side of the monitor proceeded to enter a 150-mm-diam, 300-mm-long cylindrical target chamber filled with helium gas, through a 20-mm-diam, 0.8- $\mu\text{m}$ -thick polyethylene naphthalate (PEN) window mounted on one side of the chamber. The antiprotons stopped in the helium gas, which was maintained at a temperature  $T \sim 6\text{--}30 \text{ K}$  and pressure  $p \sim 3\text{--}200 \text{ Pa}$ , and formed  $\bar{p}\text{He}^+$  atoms and  $\bar{p}\text{He}^{2+}$  ions. Differential pump-

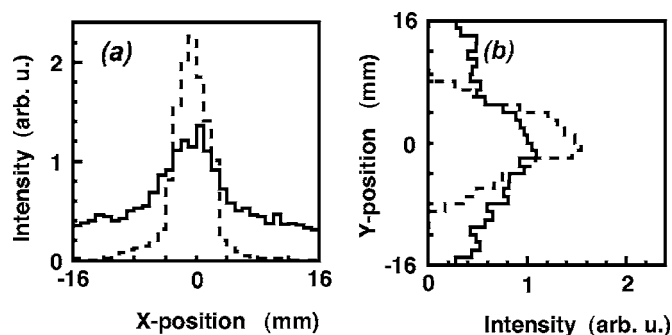


FIG. 9. The measured spatial profiles of a pulsed beam containing  $2 \times 10^6$  antiprotons (solid lines), and a laser beam of wavelength  $\lambda = 289 \text{ nm}$  (broken lines), overlapped on each other. The intensities of the two beams are independently normalized to fit on the same figure.

ing using turbomolecular pumps removed the small amount of helium permeating through the window, and so the vacuum near the monitor was maintained to better than  $p = 10^{-4} \text{ Pa}$ . Laser spectroscopy was carried out by irradiating the  $\bar{p}\text{He}^+$  or  $\bar{p}\text{He}^{2+}$  with 3–4 ns long laser pulses of energy density  $\rho = 0.01\text{--}1 \text{ mJ/cm}^2$ , their wavelengths  $\lambda = 213\text{--}726 \text{ nm}$  tuned to the atom's (or ion's) transition energies. The laser beam entered the target through a fused silica window, collinear with the antiproton beam but in the opposite direction. It then traversed the PEN window (which had optical transmissions of  $\sim 90\%$  and  $\sim 1\%$  at wavelengths  $\lambda = 400\text{--}726$  and  $213 \text{ nm}$ , respectively), and the monitor. This allowed us to measure the profiles of both antiproton and laser beams, and ensure that they were properly overlapped. In Fig. 9, the profiles of a typical pulsed beam containing  $2 \times 10^6$  antiprotons, and a laser beam of wavelength  $\lambda = 287 \text{ nm}$ , are shown superimposed on each other. The antiproton beam was found to consist of a dense core of diameter  $d \sim 10 \text{ mm}$  containing half of the antiprotons, and a halo of diameter  $d > 30 \text{ mm}$  containing the rest. Each wire electrode of the monitor intercepted between a few hundred and a few thousand antiprotons. The sensitivity of the monitor may be improved by coating the photocathode wires with e.g. cesium iodide which has a quantum efficiency several orders of magnitude higher than gold at UV wavelengths.<sup>23</sup>

## ACKNOWLEDGMENTS

The author wishes to thank the ASACUSA collaboration, R. S. Hayano, H. Klette, M. Mitani, K. Mori, W. Pirkel, T. Sekiguchi, and Y. Yamazaki. The microwire grid electrodes were developed in collaboration with the Minotos Corporation of Tokyo, Japan. This work was supported by the Grant-in-Aid for Specially Promoted Research (Grant No. 15002005) of Monbukagakusho of Japan.

<sup>1</sup>J. Peatross and D. D. Meyerhofer, Phys. Rev. A **51**, R906 (1995).

<sup>2</sup>H. T. Kim, I. J. Kim, D. G. Lee, K.-H. Hong, Y. S. Lee, V. Tosa, and C. H. Nam, Phys. Rev. A **69**, 031805(R) (2004).

<sup>3</sup>J. Krider and C. Hojvat, Nucl. Instrum. Methods Phys. Res. A **247**, 304 (1986).

<sup>4</sup>R. Fulton, J. Haggerty, R. Jared, R. Jones, J. Kadyk, C. Field, W. Kozanecki, and W. Koska, Nucl. Instrum. Methods Phys. Res. A **274**, 37 (1989).

<sup>5</sup>R. W. Alkire, E. P. Sullivan, F. D. Michaud, W. J. Trela, and R. J. Barlett, Nucl. Instrum. Methods Phys. Res. A **350**, 13 (1994).

- <sup>6</sup>J. Camas, G. Ferioli, J. J. Gras, and R. Jung, Second European Workshop on Beam Diagnostics and Instrumentation for Particle Accelerators, Lübeck-Travemünde, (DESY, Hamburg, 1995).
- <sup>7</sup>A. R. Berdoz *et al.*, Nucl. Instrum. Methods Phys. Res. A **307**, 26 (1991).
- <sup>8</sup>M. Steinacher and I. Sick, Nucl. Instrum. Methods Phys. Res. A **455**, 759 (2000).
- <sup>9</sup>S. E. Kopp, D. Indurthy, Z. Pavlovich, M. Proga, R. Zwaska, S. Childress, R. Ford, C. Kendziora, T. Kobilarcik, C. Moore, and G. Tassotto, Nucl. Instrum. Methods Phys. Res. A (to be published).
- <sup>10</sup>M. Hori, J. Eades, R. S. Hayano, T. Ishikawa, W. Pirkel, E. Widmann, H. Yamaguchi, H. A. Torii, B. Juhász, D. Horváth, and T. Yamazaki, Phys. Rev. Lett. **91**, 123401 (2003).
- <sup>11</sup>M. Hori, J. Eades, R. S. Hayano, W. Pirkel, E. Widmann, H. Yamaguchi, H. A. Torii, B. Juhász, D. Horváth, K. Suzuki, and T. Yamazaki, Phys. Rev. Lett. **94**, 063401 (2005).
- <sup>12</sup>M. Hori, Nucl. Instrum. Methods Phys. Res. A **522**, 420 (2004).
- <sup>13</sup>A. M. Lombardi, W. Pirkel, and Y. Bylinsky, in *Proceedings of the 2001 Particle Accelerator Conference, Chicago, 2001* (IEEE, Piscataway, NJ, 2001), pp. 585–587.
- <sup>14</sup>S. N. Nakamura and M. Iwasaki, Nucl. Instrum. Methods Phys. Res. A **388**, 220 (1997).
- <sup>15</sup>V. Radeka, Annu. Rev. Nucl. Part. Sci. **38**, 217 (1988).
- <sup>16</sup>T. Anderson, I. V. Tomov, and P. M. Rentzepis, J. Appl. Phys. **71**, 5161 (1992).
- <sup>17</sup>H. Henneken, F. Scholze, and M. Krumrey, Metrologia **37**, 485 (2000).
- <sup>18</sup>A. Lago, R. Wallenstein, C. Chen, Y. X. Fan, and R. L. Byer, Opt. Lett. **13**, 221 (1988).
- <sup>19</sup>R. Korde, C. Prince, D. Cunningham, R. E. Vest, and E. Gullikson, Metrologia **40**, S145 (2003).
- <sup>20</sup>I. Boscolo, P. Milani, M. Parisotto, G. Benedek, and F. Tazzioli, J. Appl. Phys. **87**, 4005 (2000).
- <sup>21</sup>F. Brandi, D. Neshev, and W. Ubachs, Phys. Rev. Lett. **91**, 163901 (2003).
- <sup>22</sup>D. Hasselkamp, H. Rothard, K.-O. Groeneveld, J. Kemmler, P. Varga, and H. Winter, *Particle Induced Electron Emission II* (Springer, Heidelberg, 1992).
- <sup>23</sup>H. Rabus, U. Kroth, M. Richter, G. Ulm, J. Friese, R. Gernhäuser, A. Kastenmüller, P. Maier-Komor, and K. Zeitelhack, Nucl. Instrum. Methods Phys. Res. A **438**, 94 (1999).